ISSN 1213-6972 (print)
ISSN 1213-6964 (online)
Journal of WSCG
http://www.wscg.eu
Vol.30, No-1-2, 2022

# 3D Point Set Registration based on Hierarchical Descriptors

Somnath Dutta
Technische Universität Dresden, Germany
somnath.dutta@tu-dresden.de

Benjamin Russig
Technische Universität Dresden, Germany
benjamin.russig@tu-dresden.de

Stefan Gumhold
Technische Universität Dresden, Germany
stefan.gumhold@tu-dresden.de

## ABSTRACT

Registering partial point clouds is crucial in numerous applications in the field of robotics, vision, and graphics. For arbitrary configurations, the registration problem requires an initial global alignment, which is computationally expensive and often still requires refinement. In this paper, we propose a pair-wise global registration method that combines the fast convergence made possible by global hierarchical surface descriptors with the arbitrarily fine sampling enabled by continuous surface representations. Registration is performed by matching descriptors of increasing resolution – which the continuous surfaces allow us to choose arbitrarily high – while restricting the search space according to the hierarchy. We evaluated our method on a large set of pair-wise registration problems, demonstrating very competitive registration accuracy that often makes subsequent refinement with a local method unnecessary.

## Keywords

3D shape registration, surface descriptors, similarity measure.

## 1 INTRODUCTION

Acquiring 3D geometry of physical objects and environments has become an integral part of numerous disciplines, ranging from applications in mechanical engineering and computer vision to asset generation for movies and games. Rapid development of 3D sensing technology over the last decades led to affordable high precision devices being widely available. Most techniques follow a sequential scanning paradigm where an object or scene is scanned from different view points. The result of this acquisition process is a set of scans, each in a local coordinate system defined by the pose of the scanning device, with different degrees of overlap. These scans have to be aligned with respect to a unique reference to obtain a final reconstructed model of an object. The accuracy of this registration step is of significant importance to the quality of the final model but is often hampered due to low-overlap between scans and inherent noise. Along with that, the registration errors may lead to artificial creases and reconstruction artifacts (oscillations or even holes).

The goal of pairwise registration is to find a transformation that aligns a source scan as close as possible to the surface represented by a target scan. The possible approach that could assist in precise registration accuracy is combination of coarse alignment followed by an iterative local refinement that results in higher convergence. The local refinement is performed effectively using variants of Iterative closest point (ICP) [Bes92] which highly depends on a good initial guess.

Coarse registration approaches usually depend on a descriptor [MPD06,Zah12,Tom10,Pet15] associated with a set of feature points encoding useful geometric information from the data based on a local neighborhood. Correspondences between descriptors are established based on similarity, resulting in a rigid transformation that best aligns the set of feature points and using some robust estimator.

The object surface is generally not sampled at the same locations between partial scans (an effect which we refer to as sampling discrepancy), and every sample is subject to measurement noise. Methods that directly rely on descriptor computation are inherently limited by these measurement issues. In addition to these external factors, methods relying on localized feature descriptors often suffer from a certain percentage of false matches, typically caused by insufficient discriminating capabilities of the descriptor and/or an underperforming similarity measure. These factors, to varying degrees, prevent them from achieving higher levels of accuracy, and the resulting rigid transformation negatively affects the convergence of local iterative algorithms employed for refinement. We propose a method that mitigates these drawbacks. Our contributions are as follows:

- novel adaption of an existing hierarchical surface descriptor to continuous surface representations
- based on that, a new pair-wise global registration pipeline for partial scans, featuring:

This work has received funding from the two DFG grants 389792660 (TRR 248, CPEC) and 390696704 (EXC 2050/1, CeTI) as well as from BMBF grant 01/S18026A-F (ScaDS.AI Dresden/Leipzig)

- high precision that compares favorably to state-of-the-art global methods
- competitive processing times
- either eliminates the need for refinement with a local method completely or gives close-to-optimal initial guesses

Additionally, the paper contributes a comprehensive evaluation of the proposed approach and compares it to the state-of-the-art global registration method by [Zho16], demonstrating measurable improvements in terms of accuracy and robustness.

## 2 RELATED WORK

Registration is a widely researched problem with vast applicability in various domains like 3D scanning, shape analysis, or motion capturing. For an overview of existing registration algorithms, we refer the reader to the respective surveys [Rus01], Salvi et al. [Sal07], Tam et al. [Tam13], Bellekens et al. [Bel14], Huang et al. [Hua21]. According to the aforementioned surveys, registration approaches can be classified with respect to the following criteria:

**Pairwise / Multi-Way.** Pairwise registration methods [Bel14] aim at registering two partially overlapping scans. Overall registration of a data set can be achieved by successively adding scans and registering them to their predecessors or to all preceding scans. On the other hand, multi-way registration [Goj09] optimizes all transforms at the same time, usually by iterating pairwise registrations or by modeling the problem with a single registration objective.

**Rigid / Non-Rigid.** Rigid registration methods [Bel14] only allow rigid body transforms for the individual scans, whereas non-rigid methods allow arbitrary ones. However, non-rigid approaches [Hua22] usually regularize the objective in order to avoid degenerate solutions (e.g. by demanding the transform to be as rigid as possible).

**Local / Global.** Local methods [Bes92, Hua11] use an initial transform estimation (e.g. provided by the user) and refine this transformation to optimize an objective. Global methods [Zho16, Pet15] do not require any input other than the geometry and find the registration transforms with arbitrary initial alignment of scans. Such global methods usually produce coarse registrations that can be refined with local methods. Furthermore these methods are not directly based on spatial proximity (but on, e.g., geometric feature descriptors).

**Learning-based Registration.** In recent years, data-driven approaches are emerging for registering point clouds primarily owing to exemplary results in both 2D and 3D applications. Researchers have used neural networks (NNs) in different ways, either to extract feature from individual point cloud followed by correspondence search or even focused on end-to-end pipeline for transformation estimation. Feature learning methods [Zen17, Hao18, Goj19] use the deep neural network to learn a robust feature correspondence search. Then, the transformation matrix is obtained by one step estimation (SVD, RANSAC) without iteration. Those NNs could provide robust and accurate correspondence searching but are fairly limited by availability of large training data and lesser generalization capabilities, resulting in a large-scale failure for unknown scenes with different distribution compared to the training data. End-to-end learning-based method [Yan19, Wan19] solves the problem of registration with complete end-to-end network, i.e, along with the correspondence search, transformation estimation is also embedded into the framework and differs from feature learning method whose focus in entirely on point feature learning. DeepGMR [Yua20] relies on a neural network to initially learn pose-invariant point-to-distribution parameter correspondences. Then, these correspondences are fed into the GMM optimization module to estimate the transformation matrix.

### Descriptors

Many 3D descriptors based on point clouds have been introduced and importantly applied to the task of point cloud registration. A comprehensive reviews for point cloud descriptors in terms of computational efficiency and accuracy are detailed in [Ale12, Guo16, Han18, Ran20, Han18]. Based on the process of descriptor extraction, the descriptors can be approximately classified as local, global, and hybrid. Local descriptors, for every point, embeds spatial distribution or geometric attributes extracted in the neighborhood and is produced by a histogram representing the descriptors for each point. It is less discriminating exactly, but suitable for cluttered scenes. Spin Image [Joh99] is a popular descriptor often used in applications of shape matching, object recognition. It creates a cylindrical support around a keypoint, divides it into radial and vertical volumes, and then counts the number of points that falls within each volume. On the other hand, a global descriptor, for the entire point cloud, is produced with a single context vector by integrating a set of features or incorporating spatial distribution of the complete data. Global-based features are generally used in 3D object recognition and object categorization, additionally some global descriptors can be used for pose estimation of the objects as they also contain local descriptors information, such as Viewpoint Feature Histogram (VFH) and Local-to-Global Signature (LGS) descriptor. Moreover, global-based methods demands less computation compared with the local features and better to describe the whole point cloud but are majorly affected by occlusions and clutter [Had14]. Hybrid-based descriptors incorporate local and global descriptors together with most of the advantages from them.

**Sampling Discrepancy**

As briefly mentioned when motivating our work in section 1, sampling discrepancy is a major factor limiting the accuracy of point cloud registration, as it means that in general, no exact correspondences can be found. Thus, many strategies have been proposed to reduce its impact. Chen and Medioni [Chen91] project points from the source shape onto their closest position in the target depth image with an iterative algorithm now known as *normal shooting* [Rus01]. The resulting point will yield an interpolated closest point on the target.

The Adaptive moving least squares (AMLS) surface based approach [Hua11] for ICP registration emphasize on the efficiency of the technique to overcome issues of sampling discrepancy. The essential concept of the AMLS method is to reconstruct a smooth and accurate representation of a surface for ICP based registration by adaptively selecting the width of a Gaussian kernel based on the principal curvature of the MLS surface through local integral invariant analysis [Yan06]. Instead of trying to minimize the distance between corresponding entities, [Mit04, Pot06] estimate the distance field of the underlying surface with local quadratic approximates and directly optimize the distance of the scan and the target surface. Kubacki et al. [Kub12] integrated multiple depth images into a model represented by implicit moving least squares (IMLS) on a grid based on signed distance function updates. Similar ideas appeared in [Par03, Mun07]. However, any such method inherently suffers from discretization artifacts at reasonable resolutions.

## 3 METHODOLOGY

The proposed method relies on the core concept of descriptor matching in order to estimate the rigid transformation. Our approach is based on the *Circon* descriptor proposed by Ferrero et al. [Car12] that represents an ordered set of radial contours around a point of interest within a point cloud. The descriptor associated with a particular point-of-interest is used to express the point cloud in a local frame. The environment around a point-of-interest is divided into sectors each representing an angle $\rho_\theta$, and are further divided radially into cells with length $\rho_r$.

The points are mapped into cells of the descriptor in a way that the cell-value represents the height (z-value) with respect to the local reference frame. Figure 1 depicts a descriptor associated with a point-of-interest (cf. section 3.1) encoding the structural information from a point cloud.

We built upon the registration method Ferrero et al. [Car12] tailored for this descriptor. While the core hierarchical approach is the same, the way they use the point cloud directly to build the descriptors ties the

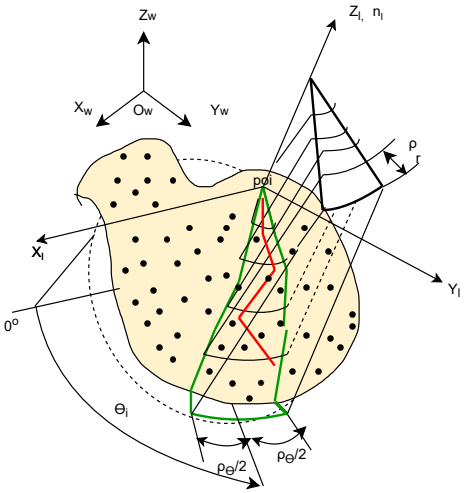


Figure 1: Descriptor spawned by a point-of-interest defining a local reference frame with cell division into sectors represented by green and red shows contour formed by maximum $z$ within each cell.

achievable accuracy to the point cloud resolution. We propose to utilize a continuous surface representation instead, enabling us to construct descriptors of arbitrarily high resolution.

The exact choice of surface representation poses a trade-off of surface expressiveness vs. computational complexity. We opted for NURBS surfaces, as their desirable properties include the ability to exactly represent relevant algebraic shapes (like ellipsoids), and many manufactured objects are likely to have been CAD-designed using NURBS originally. They also render computation of the Circon descriptor non-trivial, which required additional measures to tackle the added computational cost. Our proposed algorithm can be summarized as follows:

**AL.1** (pre-processing) Fit NURBS surfaces to the source and target point clouds.[1] We first perform Euclidean clustering [Rad09] (see **Appendix A** for details) on both to account for highly fragmented scans, and each cluster is fitted with its own surface. We refer to the union of all surfaces fitted to a point cloud as *the* surface of the point cloud.

**AL.2** (pre-processing) Sample each fitted surface at a resolution of $256 \times 256$ in parameter space to get a collection of $(u_0, v_0)$ footpoints needed later for descriptor construction (see section 3.2).

**AL.3** (pre-processing) Point-of-interest (*poi*) selection for both surfaces (section 3.1).

[1] We fit trimmed cubic surfaces using the iterative tangent distance-based refinement strategy proposed by Mörwald et al. [Moe13] as implemented in PCL [Rus11] using default parameters.

**AL.4** (pre-processing) Initial sorting of *poi* (section 3.4) pairs at a coarse resolution according to their similarity score (section 3.3), so step AL.5 can start with the most promising pairs.

**AL.5** Descriptor computation across resolutions (section 3.4) for a pair of *poi* from source and target surfaces.

**AL.6** Estimate transformation from point-pairs with highest similarity score at maximum resolution (user-defined) and evaluate stopping criterion.

**AL.7** Repeat from AL.5 until the stopping is criterion satisfied.

We elaborate on the key details of the registration methods in the following sections.

## 3.1 Selecting Points-of-Interest

Points-of-interest (*poi*) for the source and target shapes are essential for the proposed approach. They define where descriptors are initially constructed and should be chosen in a way such that the resulting descriptors cover every location on the shape at least once. The original registration algorithm by Ferrero et al. [Car12] adapts a strategy to select non-edge points by performing edge detection and thresholding based on the Laplacian of the normal vectors, essentially restricting their selection to relatively flat areas. We did not find this to provide measurable benefits, so we chose our *poi* based on a random sampling of locations on the respective surfaces to obtain the final set of points-of-interest, represented by: $s_{poi} = \{s^1_{poi}, s^2_{poi}, s^3_{poi} ..., s^m_{poi}\} \subset S$, $t_{poi} = \{t^1_{poi}, t^2_{poi}, t^3_{poi} ..., t^n_{poi}\} \subset T$, $m < N_1, n < N_2$, where $N_1$, $N_2$ are total no. of samples from the continuous surface representation of the source and target scan.

## 3.2 Descriptor Construction

Descriptors are natural choice for estimating transformation in a global registration framework as detailed in section 2. It encodes local or global structural information of a 3D shape.

The local reference frame of a Circon descriptor is defined by the normal at the point-of-interest $z_l$ (queried from the parametric surface representing the shape), some perpendicular vectors $y_l$ and $x_l = z_l \times y_l$, as well as the keypoint itself as origin. We refer to the plane with normal $z_l$ which the kepoint lies on as the *reference plane* of the descriptor.

Circon descriptors can form a hierarchy, as each cell in turn implies another keypoint that spawns a descriptor. By doubling the resolution at each level, a tree of course-to-fine representations is formed. The points-of-interest we determined in section 3.1 form roots of such a hierarchy.

So, at a given resolution, we can iterate over each valid cell $(i, j)$ of the descriptor and further build descriptors associated with the 3D point of the cell. In this regard, the descriptors are identical to [Car12], but we largely modified the construction process to work with parametric surfaces as follows: To obtain a cell value, we cast a ray from the cell along the $z$-direction of the local reference frame and compute the intersection of the ray with the surface transformed to this local frame. Since we use NURBS surfaces, the intersection has to be determined numerically as no exact analytical solution is known: We start at certain point $S(u_0, v_0)$ on the surface and optimize its position $(u, v)$ so that it lies on the ray originating from the cell center $\vec{o}$ along its direction $\hat{d}$ defined by the local frame $z$-axis. This yields the following optimization problem:

$$\underset{u,v}{argmin} \left\| (\vec{o} + < S(u,v) - \vec{o}, \hat{d} > \hat{d}) - S(u,v)) \right\|_2^2 \quad (1)$$

We use the simple Nelder-Mead algorithm [Nel65] to solve this, since the problem is low-dimensional and the evaluation of the objective function is cheap. This strategy requires an initial guess though, which we obtain in the following way:

During pre-processing, we perform a regular sampling of the NURBS surfaces in parameter space, giving us a database of footpoints on the surface and their associated parameters $(u_0, v_0)$. When transforming a surface into the local frame of the current descriptor, we can transform these footpoints along with it. Using a simple regular grid on the descriptor reference plane, descriptor cells can collect those footpoints that project close to them. We then select the most promising initial guess by applying a multi-criterion sort according to *(a)* footpoint height $z$ above the descriptor reference plane and *(b)* closeness to the ray.

We accomplish *(a)* by binning the footpoints in the cell according to their height $z$, and *(b)* results from sorting them inside each bin. For selecting the initial guess, we begin with the highest $z$-bin and choose the first (and thus, closest) sample from it. If no intersection could be found, we continue with the next sample in the bin, or the next lower bin if the current bin does not contain more samples, and so on.

The NURBS surface is then evaluated at the optimized parameter $(u', v')$ to determine corresponding 3D point along with its normal. The cell value $c_{i,j}$ is obtained from the $z$-coordinate of the point quantized with respect to a height resolution $\rho_z$ as in equation 2, i.e.

$$c_{i,j} = \lceil \frac{z}{\rho_z} \rceil \quad (2)$$

The $x$, $y$ coordinate of each cell is given by

$$\begin{aligned} x &= j * \rho_r * \cos(-(i-1) * \rho_\theta)) \\ y &= j * \rho_r * \sin(-(i-1) * \rho_\theta)) \end{aligned} \quad (3)$$

As the descriptor embeds an environment of the *poi*, it represents a closed sequence such that the first and last row is considered adjacent and also the elements with the same column index corresponds to adjacent cell. Hence, the descriptor exhibits a cyclical property that is crucial for matching and determining the rotation parameter of the alignment transformation it represents (see section 3.4).

## 3.3 Similarity Measure

There exist multiple measure, for instance, correlation coefficient, mutual information, join entropy to obtain a quantitative value and are largely dependent on the proportion of overlap area to arrive at a score. To compare the source and target descriptors for each resolution, we rely on a specific similarity measure [Car09]. In point clouds with low overlap region, it is likely that the environment around the corresponding points of source and target scan appear similar resulting in selection of false pairs. To circumvent false matching that could be detrimental to registration accuracy, the similarity measure incorporates information from the non-overlapping region enlarging its descriptive capabilities. The objective of the algorithm is to maximize similarity $S(D_s, D_t)$ in equation 5 while comparing descriptors from two surfaces. $D(s,p)$ and $D(t,q)$ refers to a descriptor with respect to point $p$,$q$ from two surfaces $s$, $t$ respectively.

$$\underset{p,q}{argmax}\ S(D(s, p \in s), D(t, q \in t)) \tag{4}$$

$$S(D_s, D_t) = \frac{\varphi_{OL}(D_s,D_t)}{(\alpha * d_{OL}(D_s,D_t)+\beta')+\varphi_{OL}(D_s,D_t)(1-\beta')} \tag{5}$$

The similarity measure $S(D_s, D_t)$ in equation 5 relies on the percentage of overlap ($\varphi_{OL}$) between two surfaces and their proximity ($d_{OL}$), representing the average distance in overlapped area. The affect of overlap in the similarity measure can be modified using $\beta'$ whereas $\alpha$ directly influences the average distance $d_{OL}$. The detailed derivation and additional concepts are provided in [Car12] and [Car09].

## 3.4 Multi-resolution Descriptor and Matching

The descriptor computation in section 3.2 and similarity measure in section 3.3 are core blocks of our hierarchical registration pipeline. The algorithm initially performs a descriptor matching at a coarse resolution of $16 \times 16$ with similarity measure described in section 3.3 between two sets of point-of-interest $s_{poi}$ and $t_{poi}$. The pairs $(s^i_{poi}, t^j_{poi})$ are sorted in decreasing order of their similarity score at this coarse resolution to obtain a feasible set of starting points for the hierarchical matching of descriptors. We try the highest-ranked pairs first, avoiding initial match ups that are unlikely to yield good results.

The actual process of descriptor comparison then works on some $(s^i_{poi}, t^j_{poi})$ pair in isolation. We name the initial pair of descriptors at some resolution the *primary* descriptors for source and target, respectively. A search is performed over each cell and its associated point on the surface of the primary source descriptor to find a *secondary* source descriptor that gives the greatest similarity to the target at some row shift $k$. This row shift represents rotation around the normal of the keypoint that spawned the secondary descriptor, determining the remaining free parameter needed to form a rigid transformation. When the rows of the secondary source descriptor had to be shifted $k$ times for highest similarity, then the rotation angle is $k\rho_\theta$, where $\rho_\theta$ is the angular step at the given resolution.

The 3D point and rotation associated with the secondary descriptor that gave the best match at the current resolution becomes the starting point for the primary descriptor at the next higher resolution. Figure 2 depicts a series of primary descriptors from coarse to fine resolution. The process terminates for a specific $(s^i_{poi}, t^j_{poi})$ pair once the specified maximum resolution is reached.

The final alignment transformation for a points-of-interest pair results from the best-matching secondary source descriptor at the highest resolution. Since we now assume both source and target descriptors to describe the same point on the surface, we can find this alignment by going from world space $W$ into the local reference frame $s$ of the final secondary source descriptor, applying the rotation resulting from the final row shift $k$, and finally concatenating the transformation back to $W$ from the reference frame $t$ of the target descriptor:

$$\mathrm{T}_{align} = {}^{W}\mathrm{T}_s^{-1} \cdot \mathrm{R}(k) \cdot {}^{W}\mathrm{T}_t \tag{6}$$

The transformation ${}^{W}\mathrm{T}_l$ for some descriptor reference frame $l$ is given directly from the keypoint $p$ that spawned the descriptor and its associated normal $n$ (see section 3.2). The rotational part of the transformation from $W$ to $l$ is obtained as follows:

$${}^{W}\mathrm{R}_l = [\vec{x}_l \quad \vec{n} \times \vec{x}_l \quad \vec{n}]^T \tag{7}$$

The full transformation ${}^{W}\mathrm{T}_l$ then follows as

$${}^{W}\mathrm{T}_l = \begin{bmatrix} {}^{W}\mathrm{R}_l & -{}^{W}\mathrm{R}_l \cdot p \\ 0_{1\times 3} & 1 \end{bmatrix} \tag{8}$$

Finally, a rotation matrix parametrized by some row shift $k$ is obtained as follows:

$$\mathrm{R}(k) = \begin{bmatrix} \cos(\rho_\theta \cdot k) & \sin(\rho_\theta \cdot k) & 0 & 0 \\ -\sin(\rho_\theta \cdot k) & \cos(\rho_\theta \cdot k & 0 & 0 \\ 0 & 0 & 1 & 0 \\ 0 & 0 & 0 & 1 \end{bmatrix} \tag{9}$$

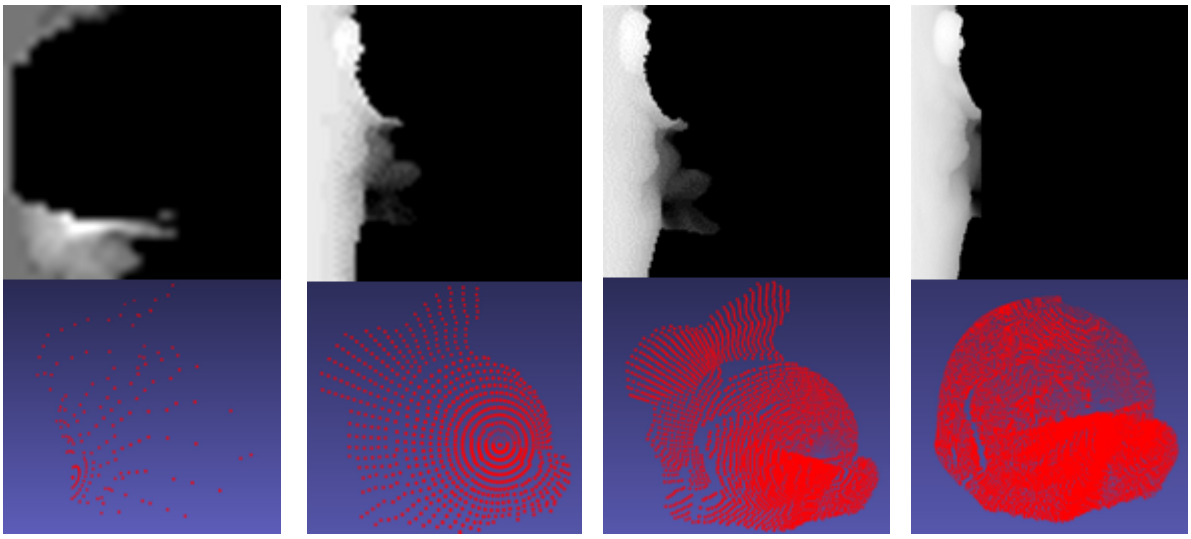

(a) 32X32 (b) 64X64 (c) 128X128 (d) 256X256

Figure 2: Descriptor cell values mapped to an image at the top and corresponding point cloud represented by the descriptor at the bottom of *Bunny* model. The restriction of higher resolution descriptors to 64 columns is visible in image *(d)*.

Our key contribution of adapting the construction of Circon descriptors to continuous surfaces enables us to extend the hierarchy with much higher resolution descriptors, without being constrained by the original resolution of the point cloud. Like [Car12], we also reduce the search space further down in the hierarchy by halving the number of columns (i.e. radial steps away from the contour center) considered at each level. This is especially important for us since descriptor computation is significantly more expensive, and there is no need to consider points far away from the center of the radial contour at later stages. To mitigate the performance impact of our construction process even further, we also limit descriptor construction to 64 columns (see figure 2d). Every cell further away than 64 radial steps will thus be invalid, which the similarity measure is able to handle naturally as part of its down-weighting of non-overlapping regions (see section 3.3).

## 3.5 Stopping Criterion

The stopping criterion is essential for the iterative search to be convergent and importantly must embed characteristics of the descriptor. To this end, we choose three non-colinear points from the final source and target descriptors that each form a triangle around the respective Circon descriptor center. Such points can be easily obtained by selecting the same three equidistantly spaced cells from the first column of each descriptor and computing their 3D point equivalents. These triangles form a fictitious correspondence pair in accordance with Ferrero et al. [Car12]. The centroid of each triangle defines a local reference frame with fictitious transformation $T_{fict}$ between them as represented by equation 6. $T_{fict}$ is compared with rigid transformation $T_{align}$ in terms of a delta transformation:

$$\Delta T = T_{align} \cdot T_{fict}^{-1} \tag{10}$$

This delta transformation is evaluated for rotational and translational difference separately (see **Appendix A** for details). If the rotational difference $\Delta r$ and translation distance $\Delta t_s$ extracted from $\Delta T$ are smaller than their respective thresholds, the algorithm terminates and $T_{align}$ is returned as the final alignment transformation.

# 4 EVALUATION

To demonstrate the effectiveness of the proposed hierarchical registration method (HER), we perform our analysis on a publicly available dataset and compare quantitative measure with state-of-the art registration method and and also the hierarchical method proposed by Ferrero et al. [Car12] and for simplicity name it as ORI−HER. We ran all our experiments on an Intel Core i5-6500 clocked at 3.20GHz. The following section presents how we performed our evaluation including dataset description and the tested methods.

## 4.1 Dataset

We performed an evaluation on the comprehensive benchmark provided[2] by Petrelli et al. [Pet15], which we refer to as the LRF dataset. This dataset contains multiple objects captured by sensors of different quality, ranging from consumer-level depth cameras to professional laser scanners resulting in point clouds with varying point density. Moreover, the benchmark includes challenging low-overlap registration pairs.

[2] http://www.vision.deis.unibo.it/list-all-categories/78-cvlab/108-pairwiseregistrationbenchmark

(a) ORI−HER (b) FGR (c) HER

Figure 3: Registration of a view-pair From LRF *OilPump* dataset

(a) ORI−HER (b) FGR (c) HER

Figure 4: Registration of a view-pair From LRF *WoodChair* dataset

## 4.2 Methods

We base our comparisons with ORI−HER [Car12] that uses hierarchical descriptors with similarity measure for coarse point cloud registration and state-of-the-art global registration method FGR [Zho16]. This methods has been shown to rival the accuracy of local methods and therefore ideal for comparison to understand the difference of accuracy with our proposed approach. The parameters for each methods and their respective values adapted during the evaluation process are described in separate **Appendix-A**.

## 4.3 Metrics

After solving the various registration problems with different methods based on the dataset discussed in section 4.1, we evaluate how well the results match the ground truth transforms with a data-dependent metric. We use root mean square error (RMSE) as a metric to quantify registration accuracy. The RMSE measures the mean error over all source cloud point locations for some computed transformation $T_{out}$ with respect to ground truth transformation $T_g$:

$$\text{RMSE}(T_{out}) = \frac{1}{\overline{d}} \sqrt{\frac{1}{n} \sum_{i=1}^{n} \|T_{out} p_i - T_g p_i\|^2} \qquad (11)$$

The normalization factor $\overline{d}$ represents the sampling distance. For the LRF dataset, where scans are represented as polygon meshes, we use the average mesh edge length.

# 5 RESULTS

The section elucidates on the results of our experiments that verify the proposed approach produces more accurate registration results than state-of-the art approach. We will also examine various characteristics of our algorithm.

## 5.1 Accuracy

The accuracy comparison is based on datasets introduced in section 4.1 with multiple registration problems and RMSE defined in section 4.3 on the registration output after convergence. We categorize RMSE results into *fine* ($< 20\overline{d}$), *coarse* ($[20\overline{d}, 50\overline{d}]$), *failed* (rest) and measure the number of view pairs (Table 1) that fall under these categories with respect to the total number of registration problems. To refine the comparison, we concentrate on the *fine* registration view-pairs and Figure 5 shows the accuracy results for the LRF datasets falling under this category. Figure 5 asserts that the highest accuracy are obtained by our method compared to FGR and ORI−HER. Furthermore, The statistical measures in Table 2 based on *fine* RMSE delineates lowest values for our method among others. The continuous representation of scans followed by descriptor computation with finer resolution attributes to the significant improvement in the accuracy. Figure 3 and Figure 4 depict particularly difficult registration problems from the LRF dataset that FGR and ORI−HER failed to align, while our method achieved *fine* alignment.

| | No.Pairs | Fine | Coarse | Fail |
|---|---|---|---|---|
| ORI−HER | 1840 | 57 | 427 | 1356 |
| FGR | 1840 | 279 | 642 | 919 |
| HER | 1840 | 355 | 711 | 774 |

Table 1: Categorization of registration view pairs from LRF datasets based on threshold as discussed in section 5.1

| | Min | Max | Avg | Std.dev |
|---|---|---|---|---|
| ORI−HER | 1.162 | 23.66 | 5.99 | 4.07 |
| FGR | 0.48 | 21.67 | 3.49 | 2.77 |
| HER | 0.34 | 20.24 | 2.58 | 2.25 |

Table 2: Statistical Comparison of RMSE based on Fine threshold as discussed in section 5.1

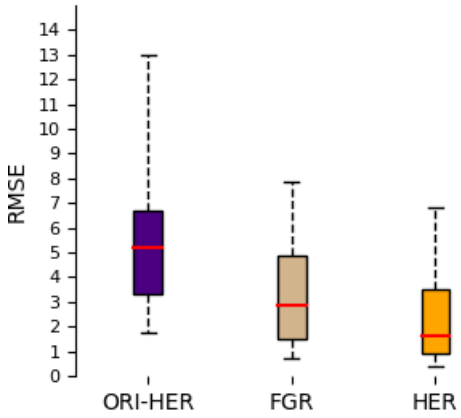


Figure 5: Accuracy comparison of pairwise registration methods for the LRF datasets. The box height represents the 25th and 75th percentile. The whiskers represent the 5th and 95th percentiles. The middle line represents the median. Better registration results are characterized by lower RMSE.

## 5.2 Runtime

We examined the computational time of ORI−HER, FGR and our approach taking into account the preprocessing steps and the core-algorithm. An analysis was performed on 10 randomly selected models from the LRF dataset. For our proposed approach, we consider three major components, i.e surface fitting, coarse resolution sorting and the iterative core algorithm. As depicted in the Figure 6, the runtime for sorting is negligible with respect to the other two components. The FGR algorithm relies on feature descriptors from a preprocessing step, which tend to be expensive to compute. Time computing the alignment is spend largely on matching these features for FGR and varies a lot depending on the point clouds. Nevertheless, it is the fastest method on average. ORI−HER exhibits the highest runtime across the comparison. We observed that it has to run through a large number of keypoint pairs (and thus, descriptor hierarchies) to determine an optimal transformation. While descriptors are significantly

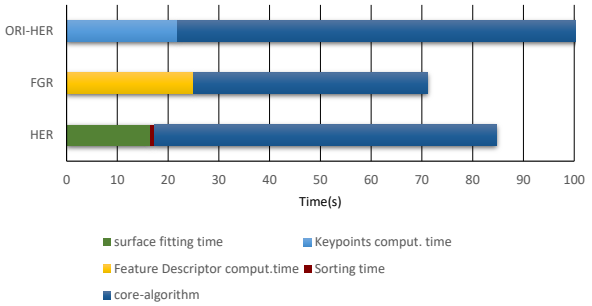


Figure 6: Runtime comparison of the proposed approach with ORI−HER, FGR including the preprocessing step for each methods. Our method exhibits higher runtime in the core algorithm part owing to its multiple descriptor computation compared to FGR but considerably lesser to ORI−HER

more expensive to compute for our method, we typically find an optimal solution within the first few keypoint pairs, as we can use higher resolution descriptors independent of the sampling situation, greatly speeding up convergence.

# 6 CONCLUSION AND OUTLOOK

In this paper, we have presented a hierarchical (coarse-to-fine) global registration method. The 2D descriptors built from a continuous representation of each point cloud enables us to embed higher accuracy into them. Our evaluation based on the diverse LRF dataset shows considerable improvement in the accuracy compared to the state-of-the-art FGR algorithm.

Nonetheless, a handful of improvements could be made, most obviously concerning speed. We chose NURBS surfaces for their versatility and ready availability of implementations, but the fitting process is expensive. Furthermore, as described in section 3.2, intersecting rays with a NURBS surface requires, in general, a numeric solution. A more specialized surface representation could accelerate both fitting and descriptor building, in turn making the use of higher resolution descriptors more feasible and thus improving accuracy even further.

Alternatively, leveraging GPU hardware to compute the descriptors promises immense speedups. This could be achieved using the programmable rasterization pipeline to generate orthographic depth maps of the continuous surfaces as viewed in the descriptor reference frame. The resolution of these depth maps can be chosen as high as needed to enable artifact-free sampling at the Circon cell centers. We expect this would bring down the computation time spend on building descriptors to a fraction of what it is in our current implementation.

# 7 REFERENCES

[Ale12] Alexandre L. A.,3d descriptors for object and category recognition: A comparative evaluation,

In Proceedings of the Workshop on Color-Depth Camera Fusion in Robotics at the IEEE/RSJ International Conference on Intelligent Robots and Systems, vol. 1, Vilamoura, Portugal, 2012.

[And01] Anderson, R.E. Social impacts of computing: Codes of professional ethics. Social Science, pp.453-469, 2001.

[Bel14] Bellekens B., Spruyt V., Maarten Weyn R. B.: A survey of rigid 3d point cloud registration algorithms. In Fourth International Conference on Ambient Computing, Applications, Services and Technologies, Proceedings, IARA, pp.8-13, 2014.

[Bes92] Besl, P. J. and McKay, N. D. A method for registration of 3-d shapes. IEEE Transactions on Pattern Analysis and Machine Intelligence 1992, 14(2):239-256

[Chen91] Chen Y., Medioni G.: Object modeling by registration of multiple range images. In Proceedings. 1991 IEEE International Conference on Robotics and Automation (Apr 1991), pp. 2724-2729

[Car12] Torre-Ferrero Carlos, Garcia Jose R. Llata, Alonso Luciano, Robla Sandra, Sarabia Esther G. :3D point cloud registration based on a purpose-designed similarity measure. EURASIP J. Adv. Signal Process. 2012: 57 (2012)

[Car09] Torre-Ferrero Carlos, Garcia Jose R. Llata, Robla Sandra, Sarabia Esther G., A similarity measure for 3D rigid registration of point clouds using image-based descriptors with low overlap. S3DV09, in IEEE 12th International Conference on Computer Vision, ICCV Workshops 2009, Kyoto, Japan, pp. 71-78 (2009)

[Goj09] Gojcic, Z., Zhou, C., Wegner, J.D., Guibas, L.J. and Birdal, T., 2020. Learning multiview 3d point cloud registration. In Proceedings of the IEEE/CVF conference on computer vision and pattern recognition (pp. 1759-1769).

[Goj19] Gojcic Zan, Zhou Caifa, Wegner Jan D, and Wieser Andreas. The perfect match: 3d point cloud matching with smoothed densities. In 16 Proceedings of the IEEE Conference on Computer Vision and Pattern Recognition, pages 5545-5554, 2019.

[Guo16] Guo Y., Bennamoun M., Sohel F., Lu M., Wan J.,and Kwok N. M., A comprehensive performance evaluation of 3d local feature descriptors, International Journal of Computer Vision, vol. 116, no. 1, pp. 66-89, 2016

[Had14] Hadji I.and De G. N., Local-to-global signature descriptor for 3d object recognition, In Proceedings of the Asian Conference on Computer Vision, pp. 570-584, Springer, 2014.

[Hao18] Haowen Deng, Tolga Birdal, and Slobodan Ilic. Ppfnet: Global context aware local features for robust 3d point matching. In Proceedings of the IEEE Conference on Computer Vision and Pattern Recognition, pages 195-205, 2018.

[Han18] Hana, X.-F.; Jin, J.S.; Xie, J.; Wang, M.-J.; Jiang, W. A Comprehensive Review of 3d Point Cloud Descriptors.arXiv 2018, arXiv:1802.02297.

[Han18a] Han X.-F., Sun S.-J., Song X.-Y., and Xiao G.-Q., 3d point cloud descriptors in hand-crafted and deep learning age:state-of-the-art, 2018, http://arxiv.org/abs/1404.3978.

[Hua21] Huang X., Mei G., Zhang J., and Abbas R. A comprehensive survey on point cloud registration. arXiv preprint arXiv:2103.02690, 2021.

[Hua11] Huang Y, Z. L., Tan Z, W. Q., and L., C. Adaptive moving least-squares surfaces for multiple point clouds registration. ASME 2011 International Design Engineering Technical Conferences and Computers and Information in Engineering Conference 2011, pages 105-113.

[Hua09] Huang, H., Li, D., Zhang, H., Ascher, U., and Cohen-Or, D. Consolidation of unorganized point clouds for surface reconstruction. ACM transactions on graphics (TOG) (2009), 28(5):176.

[Hua22] Huang, J., Birdal, T., Gojcic, Z., Guibas, L.J. and Hu, S.M., 2022. Multiway Non-rigid Point Cloud Registration via Learned Functional Map Synchronization. IEEE Transactions on Pattern Analysis and Machine Intelligence.

[Joh99] Johnson, Andrew E., and Hebert Martial. Using spin images for efficient object recognition in cluttered 3D scenes. Pattern Analysis and Machine Intelligence, IEEE Transactions on 21, no. 5 1999: 433-449

[Kub12] Kubacki, D., Bui, H., Babacan, S., and Do, M. Registration and integration of multiple depth images using signed distance function. In Computational Imaging X 2012, volume 8296,

[Lip07] Lipman, Y., Cohen-Or, D., Levin, D., and Tal-Ezer, H .Parameterization-free projection for geometry reconstruction. ACM Transactions on Graphics (TOG) (2007), 26(3):22.

[Liu06] Liu, Y.-S., Paul, J.-C., Yong, J.-H., Yu, P.-Q., Zhang, H.,Sun, J.-G., and Ramani, K. Automatic least squares projection of points onto point clouds with applications in reverse engineering. Computer-Aided Design 2006, 38(12):1251-1263.

[MPD06] Makadia A., Patterson A., Daniilidis K.: Fully automatic registration of 3D point clouds. In Proceedings of IEEE Computer Society Conference on Computer Vision and Pattern Recognition 2006)

[Mit04] Mitra, N. J., Gelfand, N., Pottmann, H., and Guibas, L. Registration of point cloud data from a geometric optimization perspective. In Proceedings of the 2004 Eurographics/ACM SIGGRAPH symposium on Geometry processing, pages 22-31. ACM.

[Moe13] Mörwald T. and Vincze M., Object Modelling for Cognitive Robotics, PhD Thesis, Vienna University of Technology, Austria, 2013

[Mun07] El Munim, H. A. and Farag, A. A. Shape representation and registration using vector distance functions. In Computer Vision and Pattern Recognition, 2007. CVPR 2007. IEEE Conference on, pages 1-8.

[Nel65] Nelder, J.A. and Mead, R. (1965), A simplex method for function minimization, Comput. J., 7, pp. 308-313.

[Par03] Paragios, N., Rousson, M., and Ramesh, V. Nonrigid registration using distance functions. Computer Vision and Image Understanding 2003., 89(2-3):142-165.

[Pet15] Petrelli A., DI Stefano L.: Pairwise registration by local orientation cues. Computer Graphics Forum 35, 2015, 59-72.

[Pot06] Pottmann, H., Huang, Q.-X., Yang, Y.-L., and Hu, S.-M. Geometry and convergence analysis of algorithms for registration of 3d shapes. International Journal of Computer Vision 2006, 67(3).

[Ran20] Ran Y. and Xu X., Point cloud registration method based on sift and geometry feature, Optik, vol. 203, Article ID 163902, 2020.

[Rad09] Rusu Radu Bogdan ,Semantic 3D Object Maps for Everyday Manipulation in Human Living Environments, PhDthesis, Computer Science department, Technische Universitaet Muenchen, Germany,2009

[Rus01] Rusinkiewicz S., Levoy M. Efficient variants of the icp algorithm. In Proceedings Third International Conference on 3-D Digital Imaging and Modeling, pp.145-152, 2001.

[Rus11] Rusu R. B. and Cousins S., 3D is here: Point Cloud Library (PCL), IEEE International Conference on Robotics and Automation (ICRA), Shanghai, China, 2011

[Sal07] Salvi J., Matabosch C., Fofi D., Forest J.: A review of recent range image registration methods with accuracy evaluation. Image and Vision Computing 25,pp 578-596, 2007.

[Tam13] Tam, G. K. L., Cheng, Z. Q., Lai, Y. K., Langbein, F. C.,Liu, Y., Marshall, D., Martin, R. R., Sun, X. F., and Rosin, P. L. Registration of 3d point clouds and meshes: A survey from rigid to nonrigid. IEEE Transactions on Visualization and Computer Graphics 2013, 19(7):1199-1217.

[Tom10] Tombari F., Salti S.,DI Stefano L.Unique shape context for 3D data description. In Proceedings of ACM Eurographics Workshop on 3D Object Retrieval 2010, pp. 57-62.

[Wan19] Wang Lingjing, Jianchun Chen, Xiang Li, and Yi Fang. Non-rigid point set registration networks. arXiv preprint arXiv:1904.01428, 2019.

[Yua20] Wentao Yuan, Eckart Benjamin, Kihwan Kim, Varun Jampani, Fox Dieter, and Kautz Jan. Deepgmr: Learning latent gaussian mixture models for registration. In European Conference on Computer Vision, pages 733-750. Springer, 2020.

[Yan19] Zhenpei Yang, Jeffrey Z. Pan, Linjie Luo, Zhou Xiaowei ,Grauman Kristen, and Qixing Huang. Extreme relative pose estimation for rgbd scans via scene completion. In The IEEE Conference on Computer Vision and Pattern Recognition (CVPR), June 2019.

[Yan06] Yang, Y.-L., Lai, Y.-K., Hu, S.-M., and Pottmann, H.Robust principal curvatures on multiple scales. In Proceedings of the Fourth Eurographics Symposium on Geometry Processing, SGP 2006, pages 223-226, Aire-la-Ville, Switzerland, Switzerland. Eurographics Association.

[Zah12] Zaharescu A., Boyer E., Horaud R.: Keypoints and local descriptors of scalar functions on 2D manifolds. International Journal of Computer Vision 100, 1 2012, 78-98.

[Zen17] Zeng Andy, Shuran Song, Niessner Matthias, Fisher Matthew, Xiao Jianxiong, and Funkhouser Thomas. 3dmatch: Learning local geometric descriptors from rgb-d reconstructions. In Proceedings of the IEEE Conference on Computer Vision and Pattern Recognition, pages 1802-1811, 2017.

[Zho16] Zhou, Q.-Y., Park, J., and Koltun, V. Fast global registration. In Computer Vision-ECCV 2016, Leibe B., Matas J., Sebe N.,Welling M., (Eds.), Springer International Publishing pages 766-782.